Respirator-Inspired Shielding and Catalytic Oxidation Strategies for Smoke-Suppression Polymers Enhancing Fire Safety

Shuai-Qi Guo [a], Lei He [a], Dan-Xuan Fang [a], Ya-Nan Wu [a], Fu-Rong Zeng [a], Ming-Jun Chen [b], Hai-Bo Zhao [a, *], Yu-Zhong Wang [a, *]

[a] *The Collaborative Innovation Center for Eco-Friendly and Fire-Safety Polymeric Materials, State Key Laboratory of Polymer Materials Engineering, National Engineering Laboratory of Eco-Friendly Polymeric Materials (Sichuan), College of Chemistry, Sichuan University, Chengdu 610064, China.*

[b] *School of Science, Xihua University, Chengdu, 610039, China.*

***Corresponding Authors**: Tel. & Fax:

E-mail: haibor7@163.com (Hai-Bo Zhao); yzwang@scu.edu.cn (Yu-Zhong Wang)

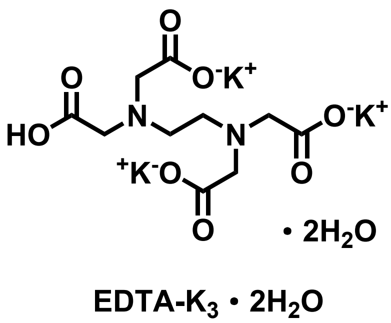

Fig. S1. Structure of EDTA-K_3•$2H_2O$

Table S1. Detailed AAS data of K element in EDTA-K_3•$2H_2O$

AAS-K element	Test value (%)	Theoretical value (%)
EDTA-K_3•$2H_2O$	27.1	26.5

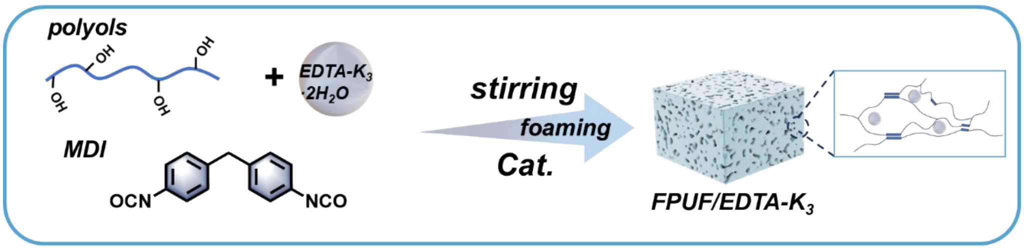

Fig. S2. Schematic diagram of the fabrication process for EDTA-K_3 filled FPUF

Table S2. Formulations of FPUF samples

Sample	DEP-330G (php)	POP-H3O (php)	H_2O (php)	TEOA (php)	DC-2525 (php)	A-1 (php)	A33 (php)	FRs (php)	MDI-2424 (php)	Denstiy (kg/m^3)
Neat FPUF	80.0	20.0	0.85	1.0	5.0	0.1	0.9	0	28.0	132±2
FPUF/15 EDTA-K_3	80.0	20.0	1.00	1.0	5.0	0.1	0.9	15	31.0	131±3
FPUF/20 EDTA-K_3	80.0	20.0	1.10	1.0	5.0	0.1	0.9	20	33.0	128±2
FPUF/25 EDTA-K_3	80.0	20.0	1.16	1.0	5.0	0.1	0.9	25	34.5	135±3

FR: flame retardant (EDTA-K_3); php: parts per hundred polyether polyols by weight.

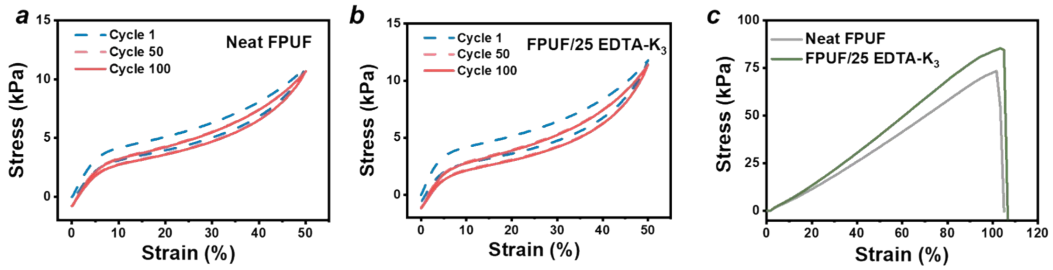

Fig. S3. Mechanical performance of flame retardant FPUF. (a-b) Compressive cyclic stress–strain curves and (c) the tensile stress–strain curves

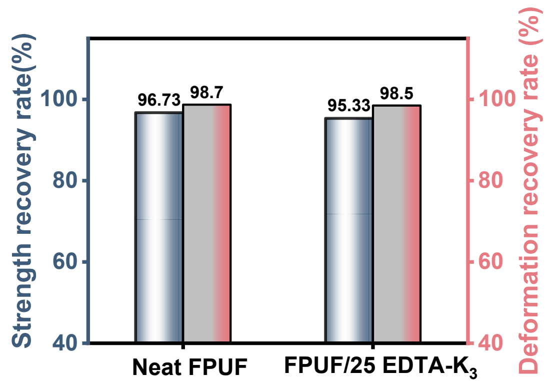

Fig. S4. Compression resilience performance of Neat FPUF and FPUF/25 EDTA-K_3.

Table S3. Results of the compression and tension tests for FPUF and FPUF/EDTA-K_3

Sample	Density (kg/m^3)	ɵ (%)	ε (%)	σ (kPa)	Toughness (kJ/m^3)
Neat FPUF	132±2	98.7±0.2	98±4	72±3	35±3
FPUF/25 EDTA-K_3	135±3	98.5±0.2	98±7	76±5	39±6

ɵ, ε, and σ represent the deformation recovery ratio, elongation at break, and tensile strength, respectively.

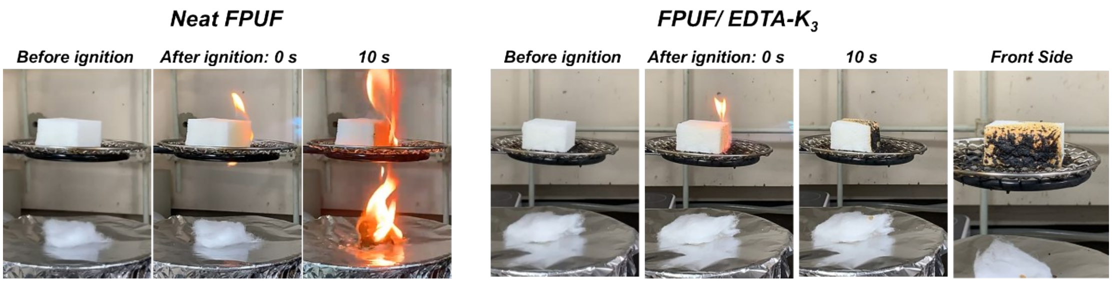

Fig. S5. Digital pictures of FPUF/EDTA-K_3 before and after the butane spray gun ignition experiment.

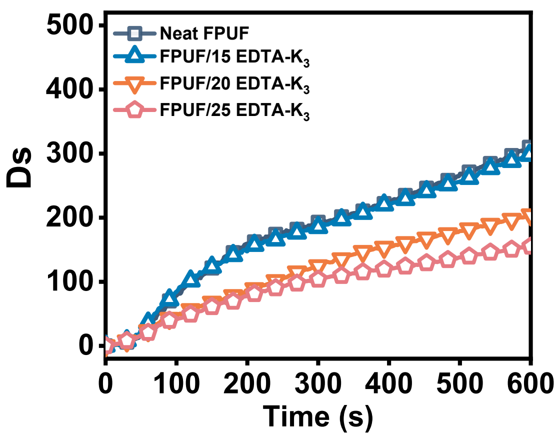

Fig. S6. Specific smoke density (Ds) for Neat FPUF and FPUF/ EDTA-K_3 with none-pilot flame mode.

Table S4. Detailed smoke test data for Neat FPUF and FPUF/EDTA-K_3.

Sample	Ds_{max}	$Ds_{max}{}^{b}$	LOI (vol%)
Neat FPUF	380±12	310±20	19.5±0.1
FPUF/15 EDTA-K_3	423±21	297±18	24.4±0.2
FPUF/20 EDTA-K_3	419±24	204±14	25.8±0.2
FPUF/25 EDTA-K_3	172±15	155±15	26.1±0.2

a: pilot flame mode; b: none-pilot flame mode

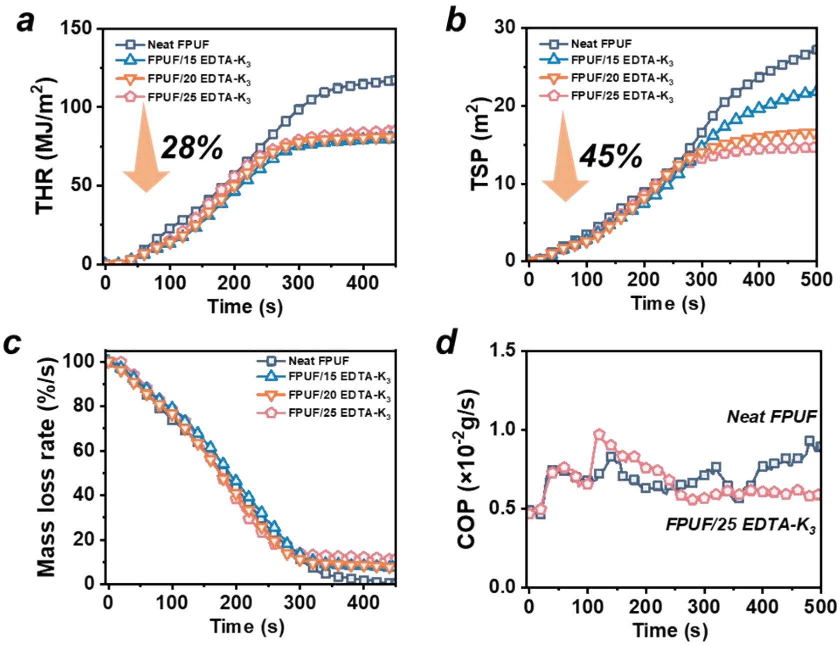

Fig. S7. Results of the cone calorimetry test for Neat FPUF and FPUF/EDTA-K_3 with varying content at the heat flux of 25 kW/m^2. (a) THR, (b) TSP, (c) Mass lose rate (MLR) curves and (d) COP.

Table S5. Detailed combustion data of Neat FPUF and FPUF/EDTA-K_3 obtained from cone calorimetry at the heat flux of 25 kW/m^2.

Sample	TTI (s)	pHRR (kW/m^2)	THR (MJ/m^2)	TSP (m^2)	char yield (%)	Av-EHC (MJ/kg)
Neat FPUF	12 ± 1	450 ± 12	118 ± 3	26.1 ± 1.1	3.2 ± 0.3	29.3 ± 1.1
FPUF/15 EDTA-K_3	10 ± 1	400 ± 22	80 ± 2	22.0 ± 1.4	8.1 ± 0.2	24.8 ± 1.2
FPUF/20 EDTA-K_3	10 ± 1	433 ± 19	81 ± 3	16.5 ± 0.4	10.6 ± 0.3	25.3 ± 0.9
FPUF/25 EDTA-K_3	10 ± 1	470 ± 23	85 ± 2	14.6 ± 1.2	11.5 ± 0.1	27.4 ± 1.5

[a]TTI: time to ignition; pHRR: peak heat release rate; THR: total heat release; TSR: total smoke release; TSP: total smoke production; Av-EHC means the average effective heat of combustion of volatiles.

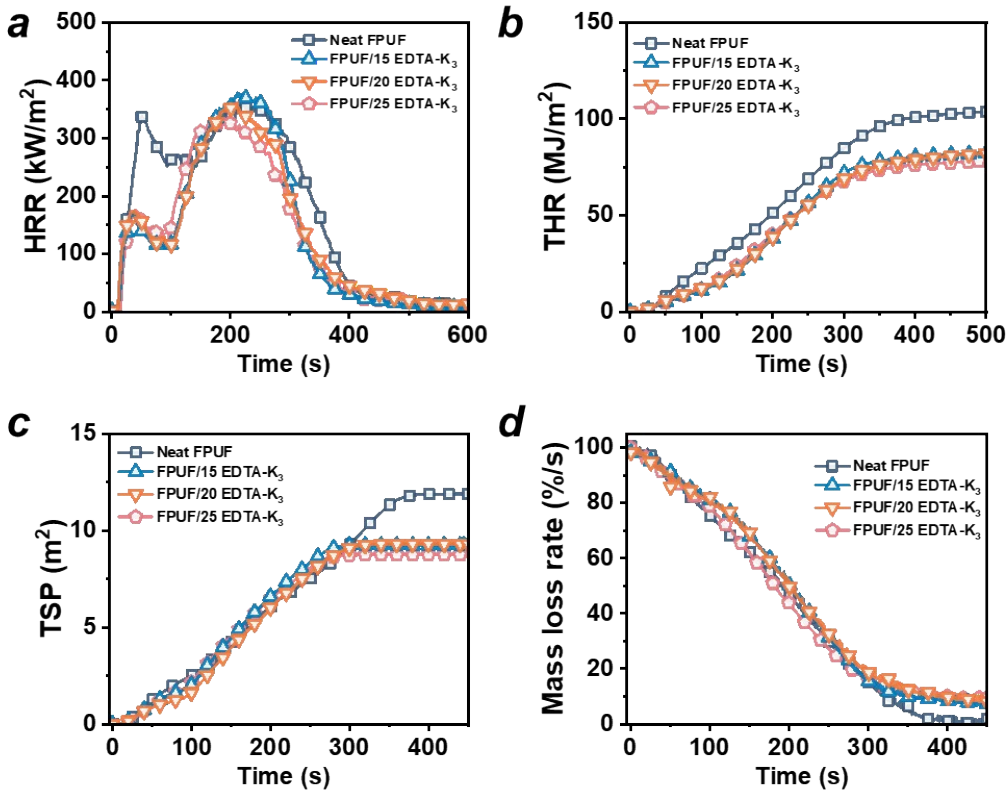

Fig. S8. Results of the cone calorimetry tests for Neat FPUF and FPUF/EDTA-K_3 with varying content at the heat flux of 35 kW/m^2. (a) HRR, (b) THR and (c) TSP curves.

Table S6. Detailed combustion data of Neat FPUF and FPUF/EDTA-K_3 obtained from cone calorimetry at the heat flux of 35 kW/m^2.

Sample	TTI (s)	pHRR (kW/m^2)	THR (MJ/m^2)	TSP (m^2)	char yield (%)	Av-EHC (MJ/kg)
Neat FPUF	11 ± 1	358 ± 12	104 ± 2	11.8 ± 1.1	4.5 ± 0.2	21.6 ± 1.1
FPUF/15 EDTA-K_3	13 ± 2	377 ± 18	83 ± 2	9.2 ± 1.8	12.2 ± 0.3	16.2 ± 0.9
FPUF/20 EDTA-K_3	12 ± 1	361 ± 10	83 ± 3	9.3 ± 1.3	13.7 ± 0.5	17.9 ± 1.2
FPUF/25 EDTA-K_3	12 ± 1	338 ± 13	78 ± 2	8.7 ± 0.5	14.5 ± 0.3	14.0 ± 1.5

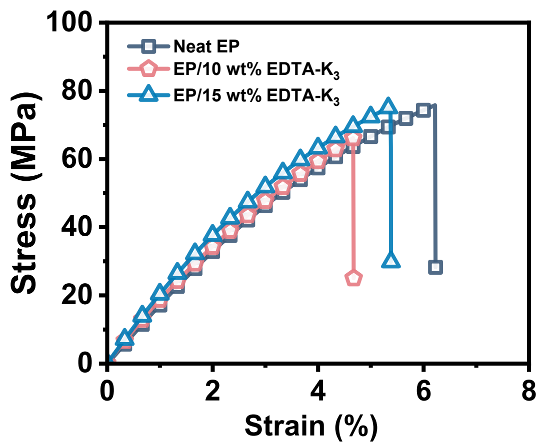

Fig. S9. Stress-strain curves.

Table S7. Mechanical properties of the EP thermosets.

Sample	Tensile strength (MPa)	Tensile Strain (%)	Tensile modulus (MPa)	Impact strength (kJ·m-2)
Neat EP	75.7±1.9	5.9±0.3	1477±31	10.0±2.4
EP/10 wt% EDTA-K_3	67.6±2.1	4.5±0.2	1565±129	10.7±1.7

EP/15 wt% EDTA-K_3	74.0±1.8	5.4±0.1	1539±104	8.2±0.5

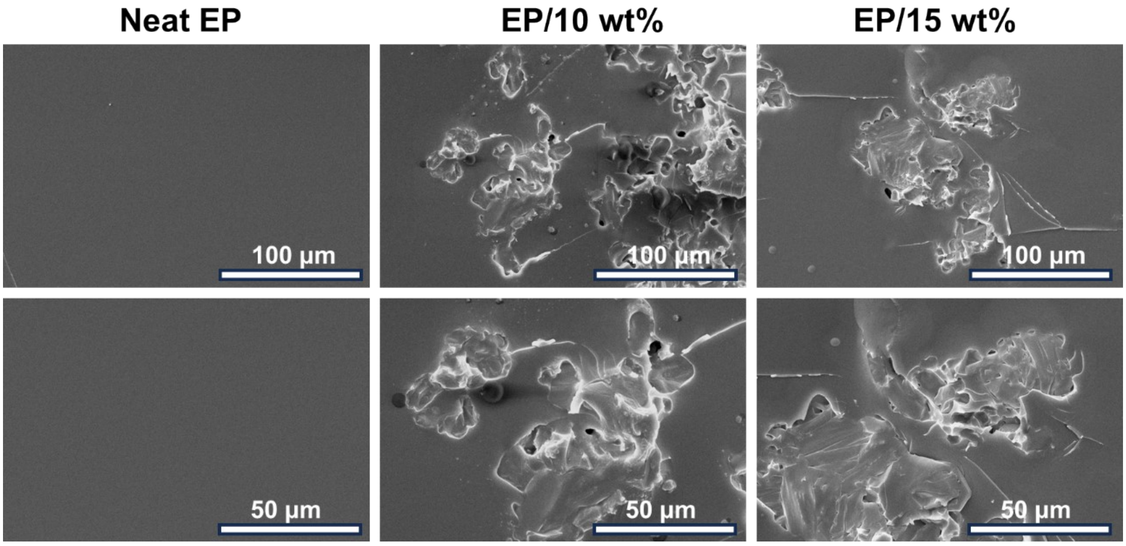

Fig. S10. SEM images of the impact fracture surface for the EP thermosets.

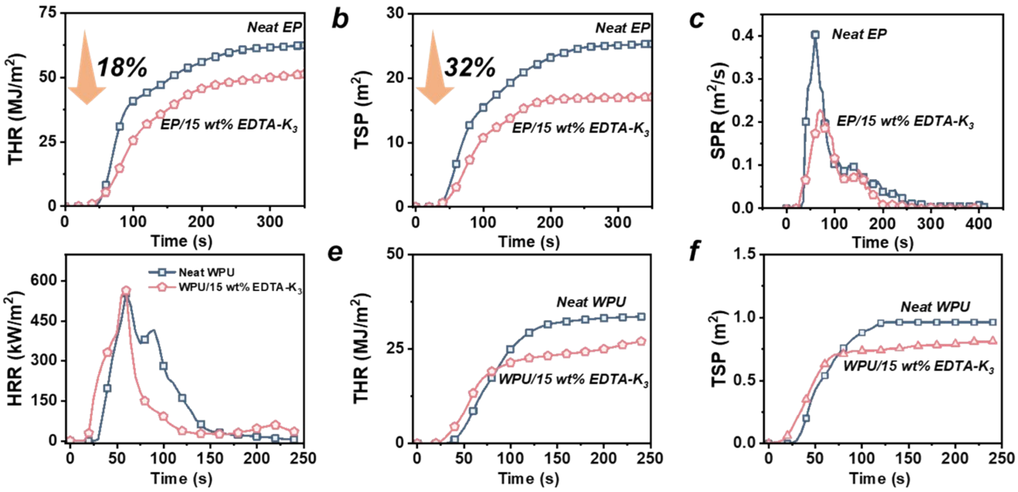

Fig. S11. Flame retardancy and smoke suppression. (a) THR, (b) TSP, and (c) SPR for EPs. (d) HRR, (e) THR, and (f) TSP for WPUs.

Table S8. Detailed data from cone calorimetry and smoke density of EPs.

Sample	TTI (s)	pHRR (kW/m^2)	THR (MJ/m^2)	TSP (m^2)	Char yield (%)	Ds
Neat EP	30 ± 1	1466 ± 22	63 ± 1	25.5 ± 1.3	6.2 ± 0.8	1320 (overrange)
EP/10 wt% EDTA-K_3	15 ± 1	960 ± 21	62 ± 2	19.0 ± 1.0	11.2 ± 1.0	941 ± 12
EP/15 wt% EDTA-K_3	20 ± 1	616 ± 18	52 ± 1	17.0 ± 0.2	13.7 ± 1.1	1002 ± 21

Table S9. Detailed data from cone calorimetry of WPUs.

Sample	TTI (s)	pHRR (kW/m^2)	THR (MJ/m^2)	TSP (m^2)	Char yield (%)
Neat WPU	25 ± 1	554±21	33 ±1	0.95±0.05	0
WPU/15 wt% EDTA-K_3	13 ± 2	564±19	27±2	0.79±0.02	1.2±0.2

Table S10. Comparisons of EDTA-K_3 with other flame retardant FPUFs

FR Structure	FR content (wt%)	LOI (vol%)	ΔTSP (%)	Cone calorimeter test condition	Ref.
EDPPA	10	21.4	+52.6	Sample size: 100×100×25 mm^3 Heat flux: 25 kW/m^2 according to ISO 5660-1:2015	[38]
	20	23.6	+74.4		
EDPPO	20	22.1	+64.6		
EDPMA	20	22.5	+71.4		
D-Urea	10	23.0	+203.7		[11]
	20	23.5	+245.5		
DMPMA	6.4	21.6	+17.6		[39]
	12.8	22.3	+24.7		
TAMPO	6.4	19.0	+19.4		

	12.8	19.4	+12.9		
BDMPP	6.4	21.5	+106		[37]
DMMP	6.4	21.0	+58		
	12.8	21.5	+63		
EDTA-K_3	15 wt.% (25 php)	26.1	-45%		**This work**

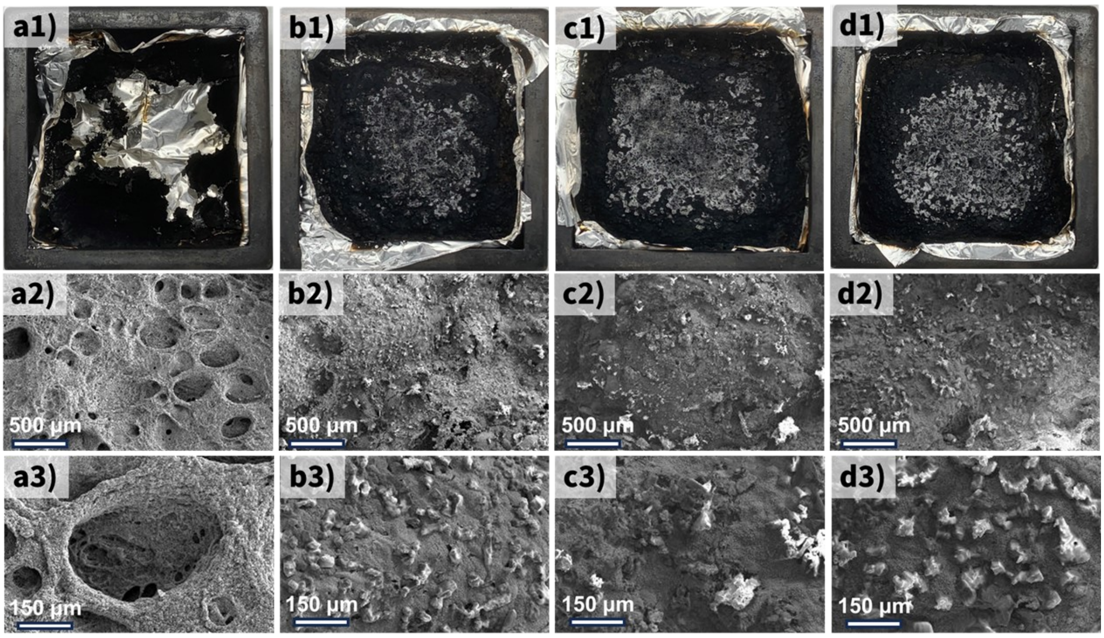

Fig. S12. Digital and SEM images of the char residues after cone calorimetry at the heat flux of 25 kW/m^2 for (a) Neat FPUF, (b) FPUF/15 EDTA-K_3, (c) FPUF/20 EDTA-K_3, and (d) FPUF/25 EDTA-K_3.

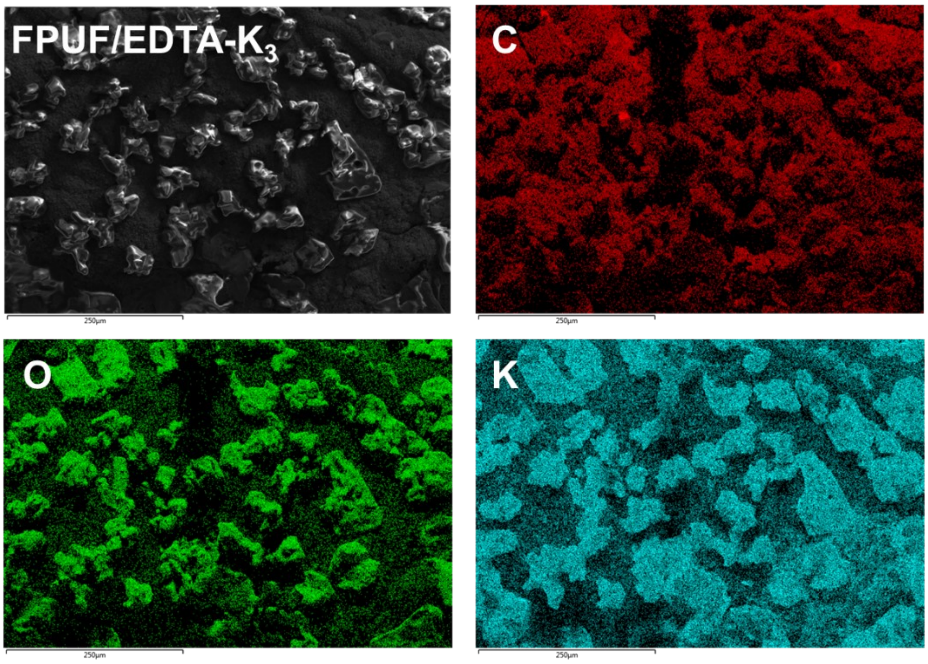

Fig. S13. SEM images for the char of the FPUF/25 EDTA-K_3 along with EDS elemental mapping.

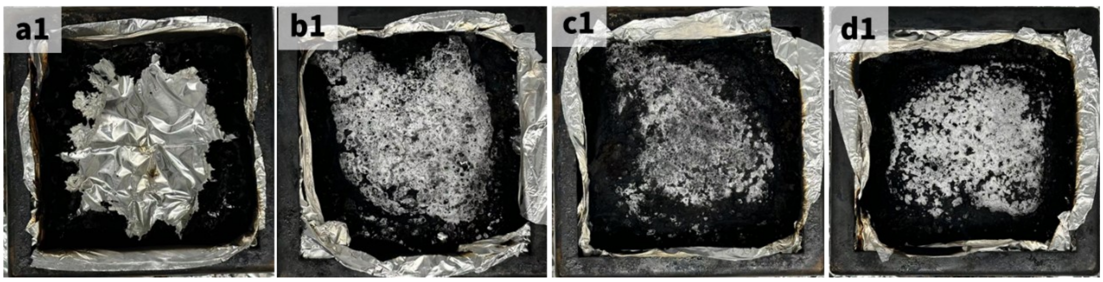

Fig. S14. Digital of the char residues after cone calorimetry at the heat flux of 35 kW/m^2 for (a) Neat FPUF, (b) FPUF/15 EDTA-K_3, (c) FPUF/20 EDTA-K_3, (d) FPUF/25 EDTA-K_3.

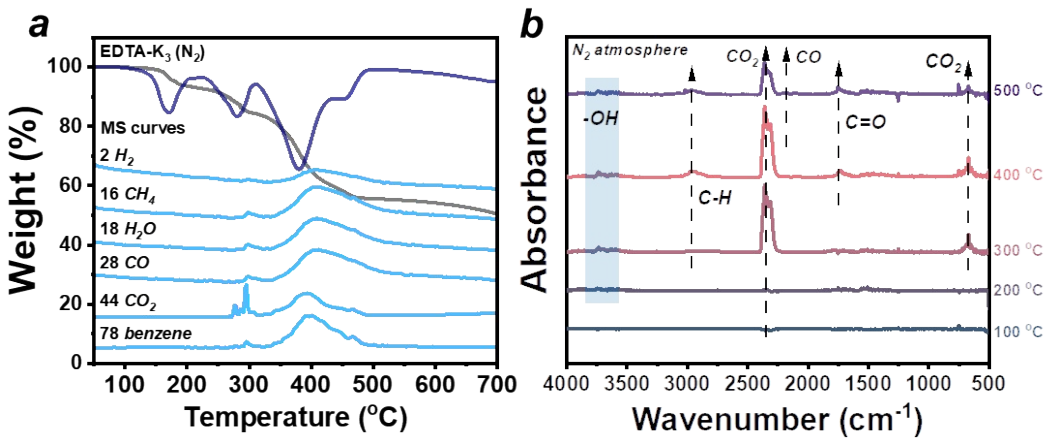

Fig. S15. TG-MS and TG-FTIR curves of EDTA-K_3 under nitrogen.

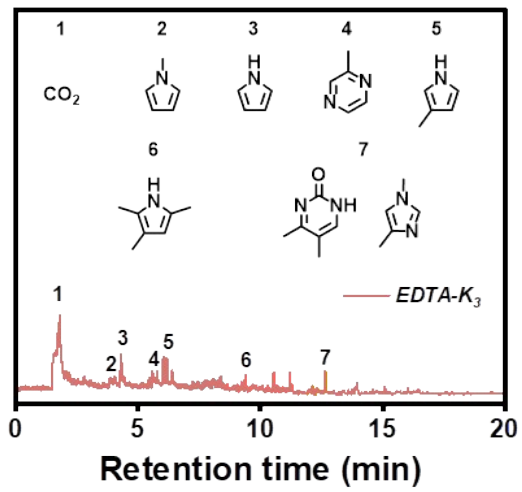

Fig. S16. Total ion chromatogram of EDTA-K_3 at 600 °C from Py-GC/MS and the main pyrolysis products.

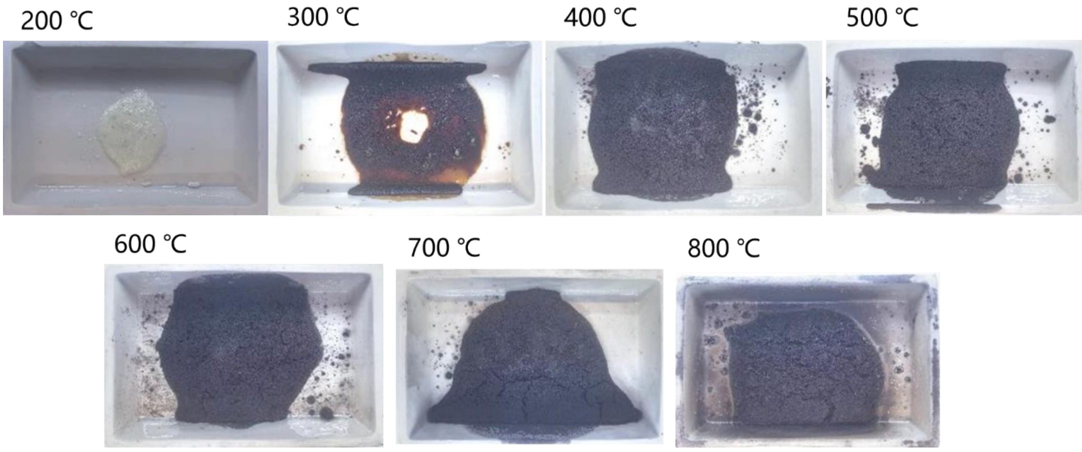

Fig. S17. Digital photos of carbon residue in tube furnace of EDTA-K_3 at different temperature.

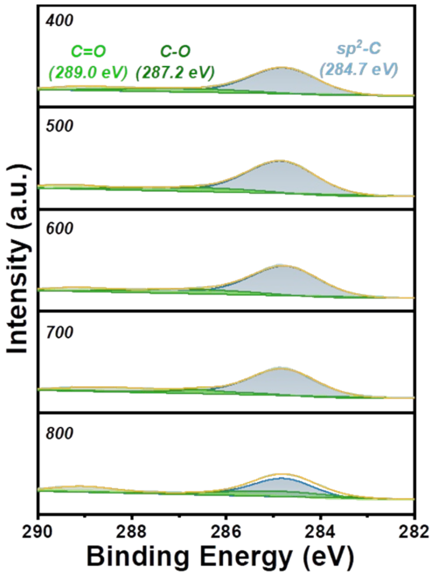

Fig. S18. High-resolution C 1s X-ray photoelectron spectra of carbons obtained from EDTA-K_3 at different temperatures.

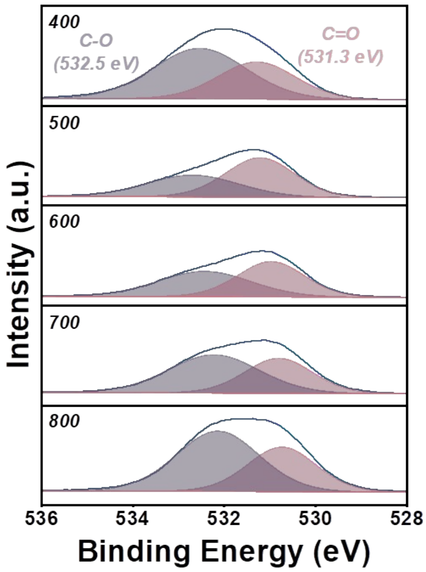

Fig. S19. High-resolution O 1s X-ray photoelectron spectra of carbons obtained from EDTA-K_3 at different temperatures.

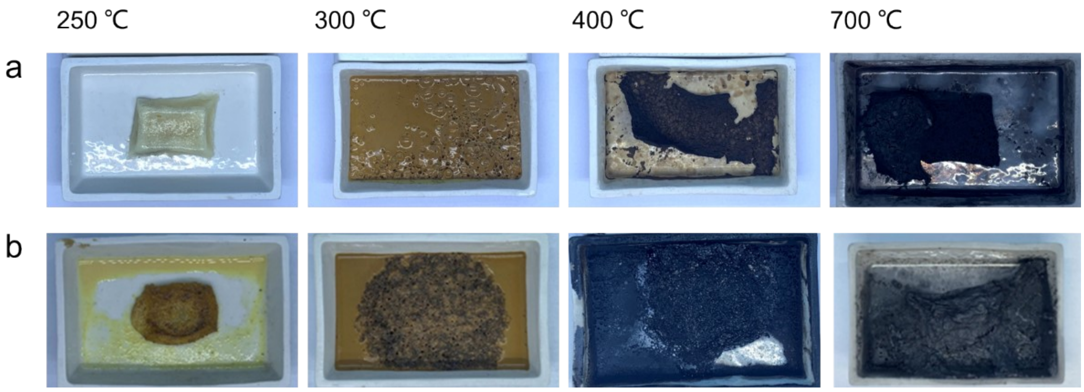

Fig. S20. Digital photos of carbon residue in the tube furnace of (a) Neat FPUF and (b) FPUF/25 EDTA-K_3 at different temperatures under nitrogen atmosphere.

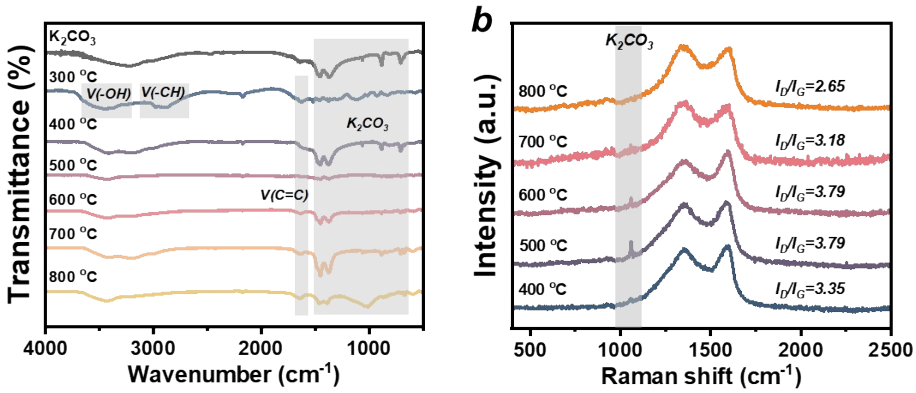

Fig. S21. Structural characterizations of the carbon residue of FPUF/EDTA-K_3 in the tube furnace under N_2. (a) Fourier transform-infrared spectra and (b) Raman spectra.

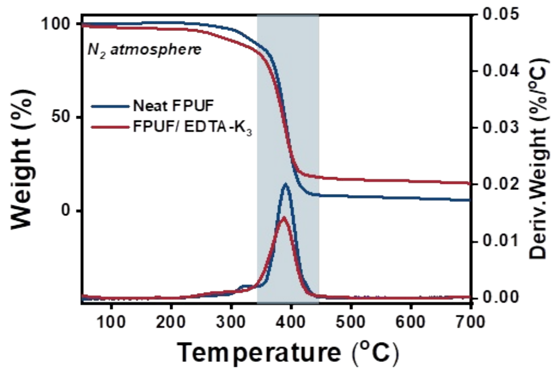

Fig. S22. TG curves of Neat FPUF and FPUF/EDTA-K_3 under nitrogen atmosphere.

Table S11. Detailed TG data of Neat FPUF and FPUF/EDTA-K_3 under nitrogen atmosphere.

Sample/N_2	$T_{5\%}$ (°C)	T_{max} (°C)	R_{max} (%/°C)	Residue (%)
Neat FPUF	315.4	390.3	2.00	5.4
FPUF/25 EDTA-K_3	265.0	387.6	1.42	11.5

Table S12. Detailed TG data of Neat FPUF and FPUF/EDTA-K_3 under air atmosphere.

Sample/air	$T_{5\%}$ (°C)	T_{max1}/R_{max1} (°C)/ (%/°C)	T_{max2}/R_{max2} (°C)/(%/°C)	T_{max3}/R_{max3} (°C)/(%/°C)	Residue (%)
Neat FPUF	275.5	330.6/1.04	357.6/1.02	531.3/0.15	0.7
FPUF/25 EDTA-K_3	249.7	326.3/1.13	487.3/0.08	-	10.1

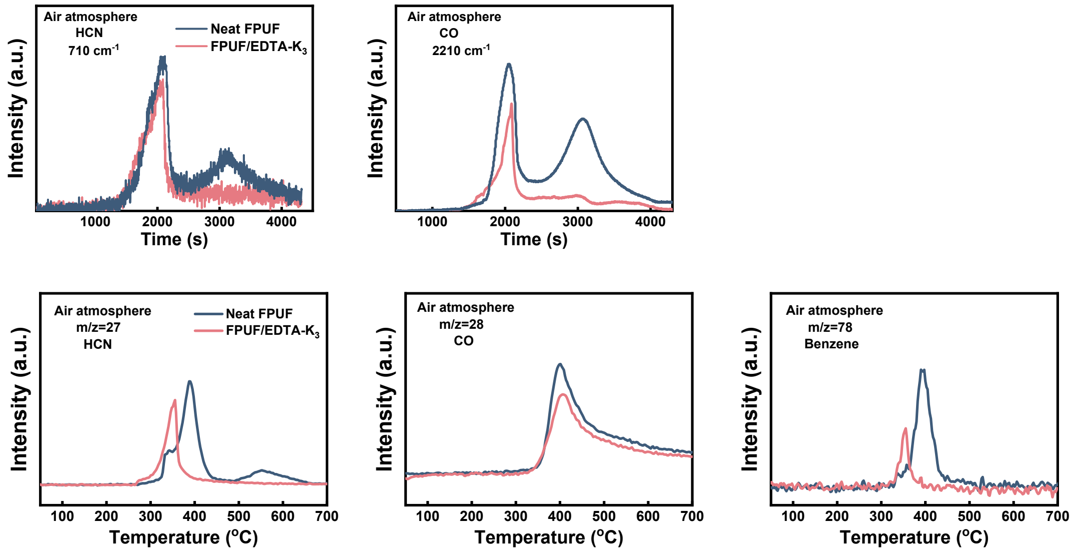

Fig. S23. TG-MS spectra of gaseous pyrolysis products of Neat FPUF and FPUF/EDTA-K_3 under air atmosphere.

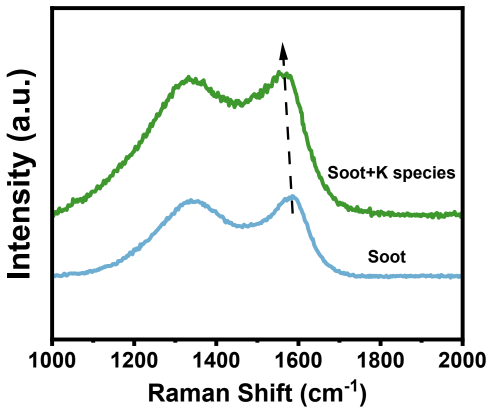

Fig. S24. Raman spectra of soot made by Neat FPUF and FPUF/EDTA-K_3.

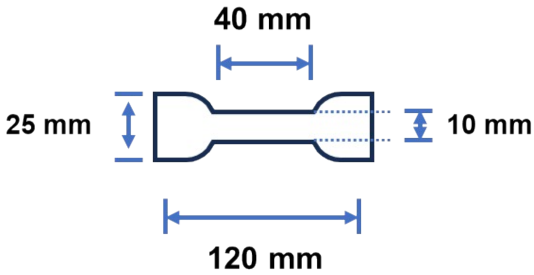

Fig. S25. Simple graphic diagram of test piece cutter for tensile measurements.